Astron. Astrophys. 270, 355–369 (1993)

ASTRONOMY AND ASTROPHYSICS

Long-term changes in emission line and continuum spectrum of the Be star γ Cassiopeiae: Hβ V/R and IR continuum flux variations

J.H. Telting[1], L.B.F.M. Waters[1,2], P. Persi[3], and S.R. Dunlop[4]

[1] Astronomical Institute Anton Pannekoek, University of Amsterdam, Kruislaan 403, NL-1098 SJ Amsterdam, The Netherlands
[2] SRON Laboratory for Space Research, p.o. box 800, NL-9700 AV Groningen, The Netherlands
[3] Instituto di Astrofisica Spaziale CNR, C.P. 67, I-00044 Frascati, Italy
[4] British Astronomical Association, Burlington House, Piccadilly, London W1V 0NL, UK

Received September 4, accepted October 5, 1992

Abstract. Long-term changes in the optical and IR continuum energy distribution of γ Cassiopeiae are compared to the variability in the line shape of the Hβ emission line. New near-IR observations are presented and combined with literature data, covering a period of 25 years. The IR data show only small variations in brightness and colour, with a trend for the K magnitude to decrease gradually. This brightening is also apparent in the V band photometry. The Hβ line profile shows the familiar V/R variations with a typical time scale of 5 ± 1 year. There is no correlation between the (strong) variations in the Hβ line profile and the strength or shape of the IR continuum.

Two models are considered that can explain the observed V/R variations: the expanding/contracting spherical shell model, and the non-axisymmetric disc model. In the spherical shell model periods of expansion give rise to a steepening of the IR continuum energy distribution because the radial density gradient of the gas increases. Conversely, periods of contraction give rise to a flattening of the IR continuum. In the disc model, no changes in the slope of the IR continuum are expected because the V/R variations are not the result of changes in the radial density gradient of the circumstellar gas.

The energy distribution of γ Cas and its variability is analysed using the S2/68 spectrophotometric data to establish the photospheric flux in the UV, and by fitting a Kurucz (1979) model atmosphere to the UV observations. The predicted optical and IR fluxes of the Kurucz model are compared to the observations in order to derive the excess emission. This excess radiation is modeled under the assumption it is due to free-bound and free-free emission from circumstellar gas.

From the comparison between the two models and the observations it is concluded that the expanding/contracting shell model cannot account for the constancy of the IR continuum, and that the non-axisymmetric disc model agrees best with the observations.

Send offprint requests to: J.H. Telting

Key words: infrared photometry – stars: Be – circumstellar matter – individual: γ Cas

1. Introduction

Be stars distinguish themselves from normal B stars by a wide range of specific properties. Among these properties are intrinsic reddening of the optical continuum, intrinsic polarization at optical and near-infrared wavelengths, and super-ionized, high-temperature, high-velocity wind regions, observed in the ultraviolet spectrum. Another well known Be-star feature is rapid rotation. Be stars show rotation velocities which are a considerable fraction of the break-up velocity. What role the rapid rotation plays in the Be phenomenon is not clear. The origin of the rapid rotation is also not known. Since centrifugal forces, due to the rapid rotation of Be stars, will ease mass loss at equatorial latitudes, dense equatorial envelopes (discs) around Be stars can be expected. Detailed reviews on Be stars are presented by e.g. Doazan (1982) and Slettebak (1988).

Compared to normal early type stars, Be stars show an excess of radiation in the IR and radio wavelength regions, caused by free-free and free-bound emission in relatively dense circumstellar matter (e.g. Gehrz et al. 1974). The matter contributing to this excess is thought to be part of a high-density, low-velocity stellar wind. The slope of the infrared and radio energy distribution of a Be star is related to the radial density distribution of such a wind. Lamers and Waters (1984) developed a method to derive the density structure of ionized circumstellar material from the observed wavelength dependence of the IR excess. Waters (1986) adapted this method and applied it to disc-like geometries. This curve of growth method, which compares observed excess fluxes with theoretical excess fluxes found by stellar-wind modelling, will be used to study the long-term changes in the continuum energy distribution of γ Cas.

Many Be stars show Hydrogen emission line profiles that are divided in two peaks, called the violet and red emission peak of the line (e.g. Doazan et al. 1987). These emission features are primarily formed by recombination in circumstellar matter. It is believed that the Hydrogen emission lines and the observed IR excess have their origin in the same region of the winds of Be stars. Dachs et al. (1986) find a clear tendency for the measured equivalent width of Hα emission lines to increase with computed envelope radii. Furthermore, Dachs et al. (1988) find a clear correlation between the IR excess and the strength of the Hα emission line.

Long-term variation in the ratio of the intensity of the violet and red Hydrogen emission peaks (V/R variation) is commonly observed in the spectra of Be stars (see e.g. Dachs (1987)). Two models that may explain this V/R variation are:

1. A star surrounded by a spherically symmetric shell which is successively expanding and contracting (e.g. Doazan 1987). In phases of expansion the emission line profiles are expected to have V/R values smaller than unity (see also Sect. 4). Phases of contraction will lead to V/R>1. Subsequent inflow and outflow phases will be accompanied by drastic changes of the radial density distribution of the wind and therefore a significant change in the slope of the IR energy distribution is expected. This implies changes in the IR colours of the star. A relation between these colours and the V/R variability as well as a relation between density parameters and V/R variability should be observed.
2. A star surrounded by a rotating non-axisymmetric, disc-like wind. If such a system is not viewed face-on, the rotation of the non-axisymmetric density distribution will cause different values of V/R (e.g. Huang 1972). Since the radial density distribution does not necessarily change in time, no change in the IR spectral index, i.e. the slope of the IR energy distribution, is expected. Hence, no relation between the V/R variability and the density structure parameters of the wind is expected. The disc-like structure could possibly be kept in its non-axisymmetric shape by tidal effects caused by a companion star or by global one-armed oscillations (Okazaki 1991). Long-term V/R variability in binary systems is indeed observed in e.g. ϕ Per, HR 2142, ζ Tau, κ Dra, HD 102567. Dachs et al. (1986) state that the shapes of measured Hα profiles are consistent with the expected shape of profiles originating in a flat differentially-rotating disc-shaped envelope. Flat equatorial envelope models have been proposed since 1931 (Struve 1931).

Both these models have to account for UV spectral features, such as observed discrete absorption components in the SiIV, CIV and NV resonance lines, which reveal the presence of a fast-outflowing, low-density wind. Hence, there must also be regions around the star where such a wind can exist. In the first model this region is placed inside the contracting/expanding shell: a spherical fast-outflowing region within the shell. In the second model the high-velocity, low-density wind is located at non-equatorial latitudes of the star.

The aim of our study is to determine the nature of the V/R variability of the Be star of γ Cas, i.e. to find out which of the above mentioned models agrees best with the observations. We will use ultraviolet, optical and infrared photometry and optical spectra, which are partly our own data and partly taken from the literature. Preliminary results are presented by Telting et al. (1991).

In the next section the star γ Cassiopeiae will be introduced. The data we used are listed and described in Sect. 3. In Sect. 4 we discuss the trends in the data. In Sect. 5 we discuss in detail the two above mentioned models which can explain the V/R variability of the star. We give a description of the way we derived the photospheric flux of γ Cas in Sect. 6. In Sect. 7 we introduce the curve of growth method which models the IR flux of γ Cas and we compare the models with our IR data. Results are discussed and conclusions are drawn in Sect. 8.

2. γ Cassiopeiae

γ Cassiopeiae was the first emission line star that was discovered (Secchi 1867) and is now one of the best studied Be stars. Its visual magnitude ($m_V \approx 2.25$) makes γ Cas, HR264, HD5394, spectral type B0.5IVe (Lesh 1968), $v\sin i$ of about 230 km/s (Slettebak 1982), the brightest Be star of the northern hemisphere. For about 100 years γ Cas has been observed in many spectral regions. The star is variable on various time scales in the optical and IR continuum, X-rays, UV resonance lines and emission lines in several spectral regions. The star has gone through shell phases and through periods of weak and strong Balmer, HeI and FeII emission (e.g. Goraya and Tur 1988). During the time span 1932–1942 γ Cas displayed spectacular variations in brightness, colour, colour temperature, line spectrum etc. After that event the brightness of the star stabilized and subsequently started to increase. The Balmer emission lines showed no V/R variation between 1946 and 1970. Since 1970 the Balmer Hβ emission line has shown a variability in the ratio of the intensities of the violet and red part (V/R) of its line profile. This cyclic variability still lasted in 1986 and has a typical time scale of 5$\pm$1 year. Similar behaviour is also seen in other Balmer emission lines. γ Cas has a varying large IR excess which is due to free-free and free-bound emission in circumstellar matter.

In 1976 γ Cas was identified as the optical counterpart of the low-luminosity, variable hard X-ray source MX 0053+604. White et al. (1982) found great similarities between the X-ray spectrum of γ Cas/MX 0053+604 and that of the X-ray pulsar X Per/4U 0352+30 (a Be and neutron star binary), and therefore concluded that the companion of γ Cas is an accreting neutron star. Results of observations of the 6.8 keV iron line made Murakami et al. (1986) suggest the presence of a white dwarf. Frontera et al. (1987) pointed out that a neutron star in a wide orbit is more consistent with the observations. No evidence for binarity of γ Cas has been found from radial velocity studies.

Simultaneous UV and Hα measurements, presented by Slettebak and Snow (1978), revealed short time scale, simultaneous variability, which correlated with an X-ray flare. Subfeatures moving trough optical HI, HeI and SiIII lines are consistent with

high-order modes of non-radial pulsations ($|m| = 12 \pm 4$) of γ Cas. Yang et al. (1988) mention a possible correlation between these subfeatures and a detected X-ray flare.

Narrow absorption components of SiIV, CIV and NV ultraviolet resonance lines are detected by Hammerschlag-Hensberge (1979) and Henrichs et al. (1983). These absorption components have central velocities ranging from -650 km/s to -1500 km/s. The appearance of discrete absorption components seems to be irregular. Doazan et al. (1987) reported that these high-velocity components appear more often and persist longer in periods when the V/R ratio of the Hβ line is larger than 1.

Recent polarization studies of γ Cas by Clarke (1990) lead to the discovery of an "intrinsic line", indicating the projection of equatorial bulges at the photosphere. This study also resulted in a deduction of the inclination angle $i \approx 45^o$.

Several detailed models for γ Cas have been developed by Marlborough (1977), Poeckert and Marlborough (1977,1978), Marlborough et al. (1978) and Scargle et al. (1978).

Mourard et al. (1989) have compared the results of their optical interferometry measurements of γ Cas with the disc model proposed by Poeckert and Marlborough (1978) which implies an inclination angle of the disc of $i \approx 45^o$. Mourard et al. conclude that the data clearly show an envelope in rotation, which approximately fits the disc model.

Waters et al. (1991) mention observations of γ Cas at $\lambda = 0.8$ mm and $\lambda = 1.1$ mm. They conclude that the radial density structure of material around the star can be represented by a power law density distribution. However, to fit the millimeter observations the power of this density law needs to be changed for large distances from the star ($R > 8\,R_*$).

3. The data

In order to investigate the nature of the variability of γ Cas, we collected ultraviolet, visual and infrared continuum observations as well as observations of the Hβ emission line. Among the IR continuum observations are observations made by one of us (P. Persi), which are never presented before. In the following we describe the collected data.

Ultraviolet continuum observations. The ultraviolet continuum observations we used are taken from the Supplement to the ultraviolet bright-star spectrophometric catalogue (Macau-Hercot 1978). The S2/68 telescope aboard the ESRO satellite collected these data of γ Cassiopeiae during two periods in 1973 and 1974. We present the UV data in Fig. 4.

After reduction the ultraviolet continuum data are dereddened by substituting the value E(B$-$V)=0.03 (Lowe et al. 1985) in the Savage and Mathis (1979) extinction curve.

Hβ observations. The Hβ data are obtained by Cowley et al. (1976) from 1969 to 1976 and by Doazan et al. (1987) from 1976 to 1986. These data are plotted in Fig. 1b.

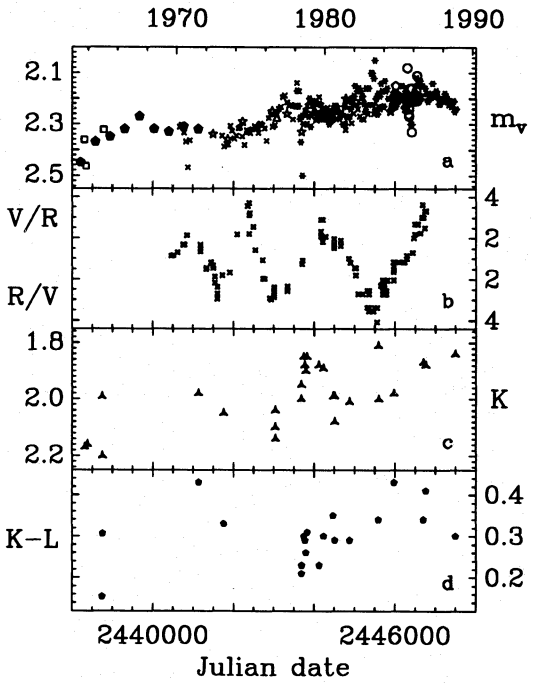

Fig. 1. **a)** Visual light curve of γ Cas. **b)** V/R behaviour of the Hβ emission line of γ Cas. **c)** K magnitude light curve based on data from Table 1. **d)** K$-$L colour magnitudes derived from data as displayed in Table 1.
Legend of Fig. 1a: dots – S.R. Dunlop and J. Isles (private communication), triangle – Ferrari-Toniolo (1978), pentagons – Böhme (1985, 1986), squares – Johnson (1966)

Visual observations. To construct a visual light curve we used observations made by members of the British Astronomical Association and the Junior Astronomical Society. These observations are eye-estimates and were made from 1963 to 1988. The observations were presented to us by J.E. Isles and S.R. Dunlop of the BAA as annual means (1963–1988), as monthly means (1978–1988) and also in a not averaged format (1970–1983) from which we calculated 50-day means (typical error in mean $\sigma = 0.1$ mag). We also used data published by Böhme (1985, 1986), Ferrari-Toniolo et al. (1978) and Johnson et al. (1966). The visual light curve is plotted in Fig. 1a. The plotted mean values of the eye-estimates display a trend of increasing brightness. The optical photometric observations are in agreement with this trend.

Infrared observations. The new infrared data, as presented in this paper, consist of 17 sets of observations made within an eleven year period. Each set contains observations simultaneously made at three or more different IR wavelengths. These data are obtained by P. Persi at Wyoming InfraRed Observatory (WIRO) and at TIRGO with both the Ge bolometer and the InSb detector. Calibration constants of the WIRO system are reported by Gehrz et al. (1974). For concise descriptions of the used TIRGO instruments see Persi et al. (1990a,1990b)

Table 1. Infrared photometry of γ Cassiopeiae. The numbers in the calibration column (C) refer to the calibration systems listed in Table 2. The reference numbers in the R column address the following papers: **(1)** Johnson et al. (1966), **(2)** Allen (1973), **(3)** Gehrtz et al. (1974), **(4)** Ashok et al. (1984), and **(5)** Waters et al. (1987). Observations without an entry in the R column have not yet been published before. The IRAS fluxes are given in erg/cm^2/s/Hz.

date		J.D.	I	J	H	K	L	M	C	R
		−2400000	mag ± 0.01	mag ± 0.01	mag ± 0.01	mag ± 0.03	mag ± 0.03	mag ± 0.05		
Oct 13	63	38316	2.357	2.481		2.17			1	1
Nov 04		38338	2.427	2.563		2.27			1	1
Dec 16		38380	2.307	2.404		2.16			1	1
Dec 13	64	38743		2.324		1.99	1.84 ± 0.05		1	1
Dec 22		38752		2.430		2.20	1.90 ± 0.05		1	1
1971					2.20 ± 0.03	1.98	1.55 ± 0.05		3	2
1972–1973 (average)						2.05	1.72	1.41	4	3
Jun 24	78	3684				2.00	1.79	1.50	4	
Jun 25		3685				1.95	1.72	1.47	4	
Aug 24		3745				1.85	1.55	1.36	4	
Sep 21		3773				1.88	1.59	1.40	4	
Oct 15		3797				1.90	1.64	1.36	4	
Nov 15		3828				1.85	1.54	1.29	4	
Sep 03	79	4120				1.88	1.65	1.29	4	
Dec 28		4236				1.89	1.59	1.14	4	
Aug 21	80	4473				1.99	1.64	1.43	4	
Sep 27		4510				1.99	1.70	1.39	4	
Oct 01		4514		2.30	2.24	2.08			1	4
Sep 30	81	4878				2.01	1.72	1.31	5	
Sep 14	83	5592				1.81	1.47	1.22	5	
Sep 20		5598		2.27	2.24	2.00		1.25	2	
Sep 30	84	5974		2.21	2.18	1.98	1.55		2	
Sep 29	86	6703		2.38	2.31	1.87	1.53		2	
Nov 27		6762		2.37	2.26	1.88	1.47		2	
Nov 25	88	7491				1.84 ± 0.04	1.54 ± 0.04	1.19 ± 0.09	5	

date		J.D.	[8.7]	N	[11.4]	[12.6]	Q	C	R
		−2440000	mag ± 0.05	mag ± 0.05	mag ± 0.05	mag ± 0.05	mag		
1972–1973 (average)			0.84	0.85	0.67	0.59	0.31 ± 0.20	4	3
Jun 24	78	3684	1.07	1.08	1.14	0.96		4	
Jun 25		3685	0.99	1.00	0.86	0.95		4	
Aug 24		3745	0.90	0.94	0.78	0.62		4	
Sep 21		3773		1.04				4	
Oct 15		3797	0.99	0.95	0.81	0.72		4	
Nov 15		3828	0.86	0.85	0.71	0.66	0.27 ± 0.20	4	
Sep 03	79	4120	0.89	0.91	0.78	0.65		4	
Dec 28		4236	0.56 ± 0.07	0.49		0.14 ± 0.15	0.09 ± 0.15	4	
Aug 21	80	4473	0.98	0.93	0.89	0.73	−0.15 ± 0.10	4	
Sep 27		4510	0.84	0.81	0.69	0.78	0.25 ± 0.05	4	
Sep 30	81	4878		0.82			−0.10 ± 0.11	5	
Sep 14	83	5592		0.59				5	
Nov 25	88	7491		0.63 ± 0.09			−0.57 ± 0.20	5	

date	log F(12 μ)	log F(25 μ)	log F(60 μ)	R
1983 (IRAS)	−21.83 ± 0.04	−22.17 ± 0.04	−22.66 ± 0.04	5

and references therein. WIRO observations are made from June 1978 to September 1980, TIRGO observations from September 1981 to November 1988.

We used additional sets of data published by Allen (1973), Ashok et al. (1984), Gehrtz et al. (1974) and Johnson et al. (1966). Far IR fluxes obtained by the IRAS satellite in 1983 (Waters et al. 1987), are also included. The data of Gertz et al. are published as means over a 13 month period. Table 1 lists all used data. Table 2 lists the calibration constants used to convert the measured magnitudes into fluxes. A K band light curve and the K−L colour history of γ Cas are plotted in Figs. 1c and 1d respectively.

According to Ashok et al. their data has to be calibrated using the Johnson calibration system. Since the original Johnson photometry system does not include H band photometry we had to calculate a H band calibration value for this system. We derived this calibration value by fitting a straight line through calibration constants for the J, K, L, M and N bands, given by Landolt-Börnstein (1982), in a C_λ versus log(λ) graph. This way we found the calibration constant for H band photometry to be C_{1650} = 19.996. The calibration constant derived by Koornneef (1983) is C_{1650} = 19.963. We did not use the calibration value given by Koornneef, because it deviates too much from the value we derived to ensure a continuous calibration value with respect to the values given by Landolt-Börnstein.

After reducing the infrared data we dereddened these data by substituting the value E(B−V) = 0.03 (Lowe et al. 1985) in the Savage and Mathis (1979) extinction curve. This extinction correction turned out to be negligible at infrared wavelengths.

4. Description of general trends

Hβ observations. In Fig. 1b the observations of the V/R ratio of the Balmer Hβ line of γ Cassiopeiae are plotted. The V/R ratio performs a cyclic variation with a typical time scale of 5 ± 1 year. This variation commenced in 1970, since when the amplitude and the period of the variation are growing. Before 1970 the V/R value was approximately equal to unity. No obvious relation between the V/R variability and the visual light curve (see Fig. 1a) can be found.

Optical observations. Optical observations of γ Cas are displayed in Fig. 1a. This figure clearly shows that the visual brightness of γ Cas is increasing throughout the years. Since 1964 the star has become ≈ 0.2 magnitudes brighter. The visual light curve given by Goraya and Tur (1988) tells us that the brightness of γ Cas has been increasing since 1940. Howarth (1979) reported measurements made in 1941 of $m_V \approx 2.8$. An increase of brightness can be due to intrinsic changes of the star itself, such as a gradual change of the effective temperature and/or the stellar radius. No observational evidence for these explanations is found. Another explanation could be that γ Cas is building up an envelope which emits the excess of radiation. To find what kind of emission mechanism can cause this flux excess, one has to construct light curves at other wavelengths to find the wavelength dependence of the flux excess.

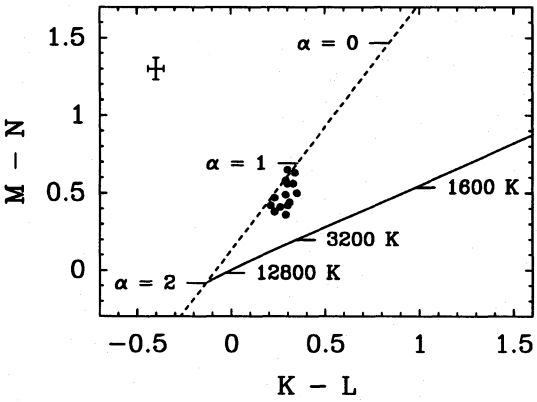

Fig. 2. M−N versus K−L colour-colour diagram of data of γ Cas. The solid line represents the position of black bodies with different temperature and the dashed line the positions of power-law energy distributions given by $S_\nu \propto \nu^\alpha$. Different values of the blackbody temperature and the power α are indicated. All data sets of Table 1 with observations in the K, L, M and N band are plotted. Typical 1σ errors of the observed colours are indicated by error bars in the upper left corner of the graph

Infrared observations. The K band light curve of γ Cas, which is plotted in Fig. 1c, shows a slight gradual brightening of the star. The curve follows the trend of the visual light curve. Since 1964 the star has become ≈ 0.3 magnitudes brighter in the K band wavelength region. In addition to the K band data from Table 1 we plotted three K band measurements of γ Cas, made by Jones (1979), in Fig. 1c.

Figure 1d displays the K−L colour history of γ Cas. All data of this plot are listed in Table 1. There seems no reason to believe that there is an increasing or decreasing trend in the K−L colour of γ Cas. Since the K band light curve follows an increasing trend, this must also be the case for the L band light curve. A comparison of Figures 1a, 1c and 1d tells us that the visual, K band and L band data of γ Cas follow a similar increasing trend.

Considering the similar increasing trends in the visual and infrared light curves, we conclude that γ Cas is storing matter, lost from the star itself, in an envelope around the star. The emission measure of the envelope is increasing with time, i.e. the envelope is getting denser and/or larger. The observed increase in flux is probably due to free-free and free-bound emission in the envelope.

The sudden appearance of the long-term V/R variability and the steady increase of the amplitude of this variability might also be correlated with the growth of an envelope. If this is the case, the beginning of long-term V/R variations might be triggered on geometrical grounds: variation starts when the envelope exceeds a certain size.

Figure 2 displays a M−N versus K−L colour-colour diagram of the data of γ Cas. The plotted colours are derived from the IR data in Table 1. The solid line in Fig. 2 represents the positions of black body energy distributions for different temperatures. The dashed line represents the positions of power-law

Table 2. Calibration constants for IR photometry. The calibration constants C_λ are used to convert data of Table 1 into fluxes in erg/cm^2/s/Hz. Fluxes are calculated using $\log F_\nu = -0.4m_\lambda - C_\lambda$. Johnson calibration constants are taken from Landolt-Börnstein (1982). The calibration constant value marked with an * is an interpolated value (see text), since originally the Johnson system has no H-band photometry.

	I	J	H	K	L	M	[8.7]	N	[11.4]	[12.6]	Q
1 Johnson	19.650	19.802	19.996*	20.200	20.562						
2 TIRGO InSB		19.786	19.963	20.177	20.597	20.770					
3 CIT			20.009	20.208	20.553						
4 WIRO				20.223	20.558	20.801	21.272	21.387	21.498	21.582	21.928
5 TIRGO bolom.				20.167	20.570	20.821		21.449			22.032

energy distributions given by $S_\nu \propto \nu^\alpha$. The plot clearly shows that the observed colours of γ Cas can not be represented by the colours predicted by any single black-body. Therefore an additional emission mechanism must be present. This mechanism is most likely free-free and free-bound emission in circumstellar matter. Free-free and free-bound emission generate a power-law energy distribution $S_\nu \propto \nu^\alpha$ with power α depending on the radial density gradient (e.g. Wright and Barlow 1975, Panagia and Felli 1975, Olnon 1975). Figure 2 shows us the value of α indicated by the IR colours of γ Cas. The indicated value of α is in agreement with that expected from free-free and free-bound emission caused by a circumstellar disc with an r^{-3} density distribution (see Sect. 7).

Figure 1 shows that the K-L colour of γ Cas did not change drastically over the period that we have observations. In particular, the strong variation in the line shape of Hβ (V/R cycles) is not seen in the optical and IR magnitudes, nor in the K-L colour. We conclude from Fig. 1 that whatever effect causes the V/R variation, it apparently does *not* produce large changes in the slope of the IR continuum. Since this slope is a measure of the radial density gradient, the conclusion seems justified that the V/R variations are not accompanied by large changes in the radial density gradient of the ionized gas.

5. Two models that may explain long-term V/R variability of Be stars and their consequences for the IR energy distribution

The shape of the Hydrogen emission lines depends on the geometry and the dynamics of the recombining circumstellar matter. Line profiles arising from moving envelopes are discussed by e.g. Sobolev (1960). Typical Hβ line profiles of γ Cas are reported by Doazan et al. (1984). In this section we discuss two models that may explain the V/R variability of the Balmer emission lines of γ Cas. In the following sections we will compare the IR colours that these models predict with our IR observations.

5.1. Spherical shell model

The first model we discuss is a star surrounded by a spherically symmetric shell with successive expansion and contraction phases. Sobolev finds that an outflowing spherical envelope can cause asymmetrical double-peaked Balmer emission line profiles with a violet peak which is smaller than the red peak, i.e. V/R<1. On the same grounds one can derive that an inflowing envelope can cause emission profiles with V/R>1. Note that to explain the observed V/R variation of the Hβ line of γ Cas infall phases lasting over at least five years are needed. Other Be stars show V/R cycles with longer quasi periods than that of γ Cas (Dachs 1987), implying even longer phases of infall.

The expanding/contracting envelope is also responsible for the large IR excess of γ Cas. The subsequent inflow and outflow of circumstellar matter implies drastic changes of the radial density distribution of the envelope. Waters (1986) points out that these changes should be accompanied by significant changes in the slope of the observed IR energy distribution. In Fig. 3 model calculations of a spherical envelope based on the radial density law $\rho(r)=\rho_0(r/R_*)^{-n}$ (see Sect. 7 or Waters 1986) are plotted. From this density law and the equation of continuity it follows that the values $n < 2$ correspond to decelerated outflow or accelerated inflow. The values $n > 2$ correspond to accelerated outflow or decelerated inflow of matter. Phases of decelerated inflow will be followed up by phases of accelerated outflow within a short time span compared to the time scales of long-term V/R variability of Be stars. Hence, decelerated inflow can only be observed at the very end of an inflow cycle. Similarly, we expect decelerated outflow only at the very end of an outflow cycle. Therefore, we conclude that, in the case of successive phases of inflow and outflow of material, in general the values of n lower than $n = 2$ represent inflow of matter and that values of n higher than $n = 2$ represent outflow of matter. Drastic changes in the slope of the IR energy distribution should be observed. In Fig. 3 the expected energy distributions for phases of inflowing and outflowing circumstellar matter are plotted.

5.2. Non-axisymmetric disc model

Another cause of asymmetrical emission line profiles may be the rotation of a non-axisymmetrical disc-like density distribution around a central object. In this model the asymmetry in the Hβ line is caused by a difference between the amount of emitting gas approaching the observer and that receding from the observer. The V/R variability is caused by the gradual change of each of these amounts. We consider the simple case of a rotating disc with a high-density part and on the opposite side of the star a low-density part. Individual particles circle through this

slowly-rotating density pattern. If we do not see this disc face-on, we expect to find V/R values greater than unity if the high density part of the envelope, where most of the Balmer emission is formed, is moving towards the observer. Consequently, if the high-density part is receding from the observer, we expect emission line profiles with V/R<1. The non-axisymmetric shape of the disc might be due to tidal effects of a (low mass) companion. Another explanation of this effect might be the existence of global m=1 modes in the disc (Okazaki 1991). The same V/R behaviour can be expected in the case of a slowly rotating, homogeneous elliptically shaped disc with the star in a focal point.

Since the radial density distribution does not necessarily change much in time, no change in the IR spectral index is expected. As found for many Be stars a value of $n \approx 2-3$ can be expected (Waters et al. 1987).

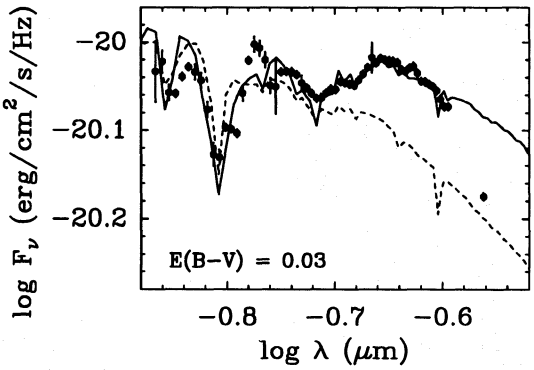

Fig. 4. S2/68 data with fitted Kurucz models. We used E(B−V)=0.03 to deredden the data. **Solid curve**: Fitted Kurucz model with parameters T_{eff} = 22500 K and log g = 3.0. Spectral fit range: 135–275 nm. **Dashed curve**: Fitted Kurucz model with parameters T_{eff} = 30000 K and log g = 3.5. Spectral fit range: 135–200 nm

6. Photospheric flux

6.1. The photospheric flux of γ Cas

In Sect. 7 we will compare the IR excess fluxes of γ Cassiopeiae with modelled IR excesses. In order to reduce photometric IR observations to excess fluxes one has to subtract the photospheric flux from the measured fluxes. To find the photospheric flux we fitted Kurucz (1979) models, with solar abundances, to our ultraviolet continuum data of γ Cas. The ultraviolet flux finds its origin in the stellar photosphere. A high-density, disc-like or spherical wind is believed not to contribute significantly to the stellar (far) UV flux and therefore the total UV flux is not affected significantly by variations in this wind. We assume the ultraviolet flux to be constant.

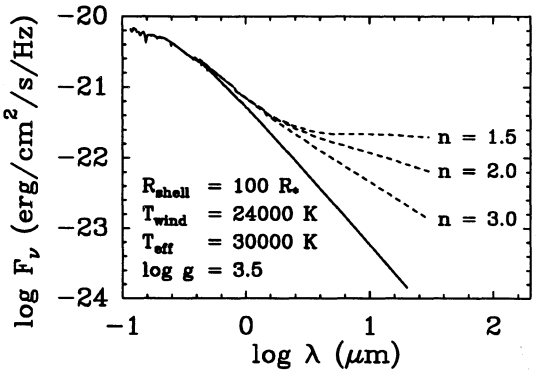

Fig. 3. Model calculations of the effect of changing the density gradient (parameter n) of a spherical envelope (dashed curves). The IR excess is caused by bound-free and free-free emission. Note the slopes of the energy distribution for different values of n. If $n > 2$ the matter in the envelope is flowing outwards. Inflow of matter should result in a much shallower slope of the IR density distribution (in this case n = 1.5 is used). The solid curve is a Kurucz model with parameters T_{eff} = 30000 K and log g = 3.5

The S2/68 data spectrum ranges from 136 to 274 nm. Because the influence of excess fluxes due to a circumstellar wind increases from the shorter to the longer end of this wavelength range (see next section), we fitted Kurucz models to all available ultraviolet data and also to the shorter half of our ultraviolet data spectrum (135–200 nm). The results of this fitting procedure show that different Kurucz models qualify as best fits for these spectral ranges. Therefore the entire S2/68 UV flux spectrum of γ Cas can not be ideally represented by one of the Kurucz models. Hence we decided to analyse and model our IR data for two cases; the first based on a photosphere model fitted to the wavelength range 135–275 nm, the second based on a photosphere model fitted to the range 135–200 nm. In the first case we chose the best-fitting Kurucz model, being the one with T_{eff} = 22500 K and log g = 3. To test the influence on our results of the use of different Kurucz models as representations of the photospheric flux, we used in the second case the model with T_{eff} = 30000 K and log g = 3.5. In both cases the IR and far IR data were reduced to excess fluxes by subtracting the, to corresponding wavelengths interpolated, Kurucz fluxes. Figure 4 shows the adopted Kurucz models fitted to the S2/68 data of γ Cas. Table 3 lists the results of fitting Kurucz models to our ultraviolet data of γ Cas. The fitting of Kurucz models to the UV energy distribution of γ Cas is also performed by e.g. Goraya and Tur (1988) and Waters et al. (1990). The former use models with T_{eff} = 17000 K, log g = 4 and T_{eff} = 27000 K, log g = 4, the latter use the model with T_{eff} = 25000 K, log g = 3. Furthermore, the value T_{eff} = 25000 K is adopted by Poeckert and Marlborough (1978) for their model of γ Cas.

When the best-fitting Kurucz model, which represents the photospheric flux, is found, it is possible to derive the intrinsic visual magnitude of the star, i.e. the visual magnitude expected if there were no envelope present. Table 3 also lists the visual magnitudes predicted by these Kurucz models. These visual magnitudes have to be compared to the observed value $m_V \approx 2.8$ (Howarth 1979), which was the visual magnitude of γ Cas after its shell ejecting phase. Since this value of m_V is seen with

Table 3. Results of fitting Kurucz models to the UV fluxes of γ Cas. Temperatures are given in Kelvin, fluxes are given in erg/cm^2/s/Hz. For each spectral fit range the fit column ranks the fitted Kurucz models according to the quality of the fit. Visual magnitudes are calculated using $m_V = -2.5\,(C + \log F_{Kur}\,(550))$, with C = 19.436 (Landolt-Börnstein 1982). Interpolated models are indicated with an *.

	Fit range	$135 \leq \lambda \leq 200$ nm.		
T_{eff}	log g	fit	log $F_{Kur}(550)$	$m_{V,Kur}$
22500	3.0	2	−20.362	2.32
25000	3.0	1	−20.457	2.55
27500*	3.5	4	−20.537	2.75
30000	3.5	3	−20.604	2.92
32500*	3.5	5	−20.633	2.99
35000	3.5	6	−20.660	3.06

	Fit range	$135 \leq \lambda \leq 275$ nm.		
T_{eff}	log g	fit	log $F_{Kur}(550)$	$m_{V,Kur}$
22500	3.0	1	−20.363	2.32
25000	3.0	2	−20.450	2.54
27500*	3.5	3	−20.511	2.69
30000	3.5	4	−20.571	2.84

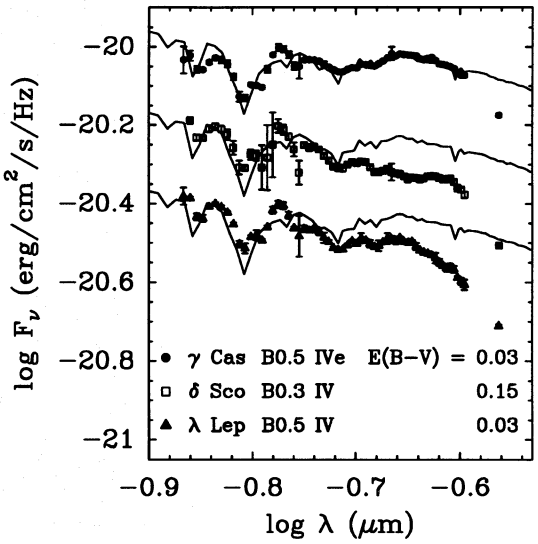

Fig. 5. Comparison of the UV energy distribution of γ Cas with the energy distributions of δ Sco and λ Lep. The energy distributions of δ Sco and λ Lep are shifted in log(Flux) direction for convenience. A Kurucz model (T_{eff} = 22500 K , log g = 3) is fitted to the S2/68 data of the stars. The spectral range to which the model is fitted is 135–200 nm. Note that the slope of the energy distributions of δ Sco and λ Lep is much steeper than the slope of the energy distribution of γ Cas

practically no matter surrounding the star, it can be considered as the best estimate for the photospheric visual magnitude at that time (1941). The photospheric magnitude should still be the same if the increase in visual magnitude that is displayed in Fig. 1a is caused only by circumstellar emission, and not by intrinsic changes of the star. Although the Kurucz model with T_{eff} = 22500 K fits the ultraviolet data better than the model with T_{eff} = 30000 K, the results in the m_V columns of Table 3 point out that the latter model agrees better with the observed value of the intrinsic visual magnitude.

The photometric data of γ Cas are dereddened by substituting the value E(B−V) = 0.03 in the Savage and Mathis interstellar extinction law. This value of E(B−V) might be inaccurate. Since circumstellar matter around γ Cas reddens the intrinsic flux of the star, the value of E(B−V) in the direction of γ Cas is hard to derive. Adopting a different value of E(B−V) would change the shape of the resulting dereddened energy distribution. This could lead to different best-fitting Kurucz models. This effect, however, hardly affects the slope of the resulting IR excess, and therefore we conclude that the accuracy of the adopted value of the interstellar extinction serves the purpose of this study well.

6.2. Comparison with B0.5 type stars

We compare the ultraviolet energy distribution of γ Cas with the energy distribution of two B type stars, to check the validity of the best-fitting Kurucz model for γ Cas. The two comparison stars are δ Sco, HR5953, B0.3IV, $v\sin i \approx 181$ km/s and λ Lep, HR1756, B0.5IV, $v\sin i \approx 67$ km/s (Hoffleit and Jaschek 1982). We used S2/68 UV observations of δ Sco and λ Lep and applied interstellar extinction values E(B−V) = 0.15 and E(B−V) = 0.03 respectively. The ultraviolet energy distributions of the three stars are plotted in Fig. 5. A Kurucz model with parameters T_{eff} = 22500 K and log g = 3 is fitted to the observations with $135 < \lambda < 200$ nm. Figure 5 clearly shows that, although the three stars have the same spectral type, the UV energy distributions of δ Sco and λ Lep are much steeper than the energy distribution of γ Cas. These steeper energy distributions are consistent with photospheric temperatures that are higher than the effective temperature of the best-fitting Kurucz model of γ Cas. Therefore the above derived photospheric effective temperature T_{eff} = 22500 K of γ Cas might be too low and the use of an effective temperature of T_{eff} = 30000 K seems justified. Furthermore, the energy distribution of γ Cas seems similar to the ones of the comparison stars for $\lambda < 175$ nm. At longer wavelengths γ Cas displays an excess of flux in comparison with δ Sco and λ Lep. These properties of γ Cas can be due to circumstellar flux contribution or to a different effective temperature at lower latitudes caused by rapid rotation. The first of these possibilities is probably correct.

We conclude that the effective temperature of γ Cas must be higher than T_{eff} = 22500 K. As mentioned before, we will use the Kurucz model with T_{eff} = 22500 K and log g = 3 to model the photospheric flux of γ Cas. In addition, we will process our data with the Kurucz model with T_{eff} = 30000 K and log g = 3.5 as a model for the photospheric flux. Results of both analyses will be given in the next section.

7. Modelling and fitting the IR excess

7.1. The curve of growth model

The IR excess caused by free-free and free-bound emission in a disc around a star can be modelled with the curve of growth (COG) method (Waters 1986). In the following we will discuss this COG method, closely following the presentation given by Waters. For simplicity the following assumptions are made:

- The disc is viewed pole-on.
- The disc is isothermal ($T_{disc} = 0.8 * T_{eff}$).
- The IR flux finds its origin in both star and disc.
- Matter in the polar stellar wind does not contribute to the total IR flux.
- The density distribution is given by

$$\rho(r) = \rho_0 \left(r/R_*\right)^{-n} \qquad \wedge \qquad r > R_* \tag{1}$$

where ρ_0 is the density of the disc at the photosphere and R_* is the stellar radius.

- The disc has a finite radius R_{disc}. Therefore the density distribution is a function of n, R_{disc} and the opening angle of the disc.

The optical depth along a line of sight through the disc can be written as

$$\tau(q) = E_\nu * f(n, q, \theta) \tag{2}$$

where f(n,q,θ) is a function of the disc geometry, n the exponent of the density law, q the impact parameter of the line of sight, given in units of R_*, and where θ is the opening angle of the disc. COG models give the excess flux as a function of the optical depth parameter E_ν. This optical depth parameter is defined as

$$E_\nu = X_* * X_\lambda \tag{3}$$

with

$$X_* = 4.923 * 10^{35}\ \overline{z^2}\ T_{disc}^{-3/2}\ \mu^{-2}\ \gamma\ \rho_0^2\ R_* \tag{4}$$

containing only stellar and disc parameters and with

$$X_\lambda = \lambda^2 \left(kT_{disc}/h\nu\right) \left(1 - e^{-h\nu/kT_{disc}}\right) * \left\{g\left(\nu, T_{disc}\right) + b\left(\nu, T_{disc}\right)\right\} \tag{5}$$

depending on the considered wavelength λ and the disc temperature T_{disc}. In Eqs. (4) and (5) λ stands for the wavelength in cm, ν for the frequency in Hz, g(ν,T_{disc}) and b(ν,T_{disc}) for the gaunt factors for free-free and free-bound emission respectively, $\overline{z^2}$ for the mean value of the squared atomic charge, γ for the ratio of the number electrons to the number of ions, μ for the mean atomic weight in units of proton mass, R_* for the stellar radius in $R_\odot$, T_{disc} for the disc temperature in K and ρ_0 stands for the density in g/cm^3 at the base of the disc (r=R_*). Parameters $\overline{z^2}$, μ and γ apply to the matter in the disc.

The excess flux is written as $Z_\nu - 1$, where Z_ν stands for the monochromatic flux ratio

$$Z_\nu = \left(F_{\nu,*} + F_{\nu,disc}\right) / F_{\nu,*}. \tag{6}$$

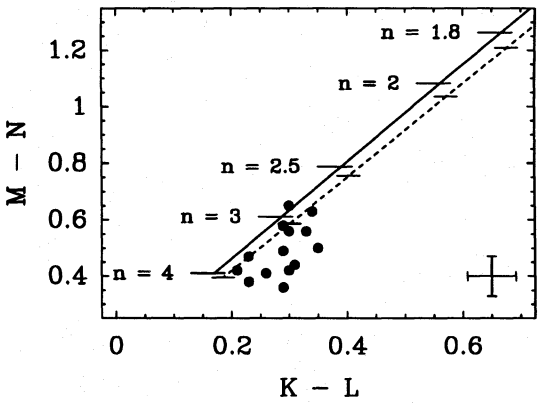

Fig. 6. M−N versus K−L colour-colour diagram of data of γ Cas. The dashed and solid lines represent model calculations based on a power-law density distribution for stellar parameters T_{eff} = 22500 K, log g = 3.0 and T_{eff} = 30000 K, log g = 3.5 respectively. Different values of the density parameter n are indicated. All data sets of Table 1 with observations in the K, L, M and N band are plotted. Typical 1σ errors of the IR colours are indicated by the error bars in the lower right corner of the graph. Note the position of the data points with respect to the indicated values of n. No points that correspond to values of $n < 2$ are found, i.e. no infall of matter is expected

A typical curve of growth model can be divided into an optically thin, a partially optically thick and an opaque region. If, for a given wavelength, the whole disc is optically thin, the resulting excess flux is proportional to the emission measure, i.e. proportional to $n_e * n_p$ integrated over the volume of the disc (with n_e as the electron density and n_p the density of the ions participating in the free-free and free-bound emission processes). If the whole disc is optically thick, the star + disc radiate like a black body with a radiating surface of πR_{disc}^2. The slope of the curve is zero and the excess flux ratio is independent of wavelength. In the partially optically thick case, for a given wavelength, the inner parts of the disc are optically thick while the outer parts of the disc are optically thin.

The shape of the curve gives information about the density structure parameters (Eq. (1)). The slope of the curve in between the optically thin and thick turnover points is determined by the exponent n in the density law. The position of the optically thick turnover point depends on the adopted disc radius R_{disc}. The models are shifted horizontally in a log($Z_\nu - 1$) versus log(E_ν) diagram (see Fig. 7) to fit the IR excess fluxes. This shift yields the parameter X_* from which the density of the disc at the stellar photosphere ρ_0 can be derived, provided the stellar and disc parameters (Eq. (4)) are known.

The opening angle θ of the disc does not greatly affect the shape of the curve of growth. Increasing the opening angle of a COG model, would simply shift the curve to the left end of the log($Z_\nu - 1$) versus log(E_ν) diagram. Hence, fitting COG models with different opening angles will result in different horizontal shifts, i.e. different values of ρ_0.

The slope of the partially optically thick part of the curve of growth is, besides of the value of n, also affected by a possible temperature gradient and by the disc geometry. These quantities,

Table 4. χ^2 values as a function of degrees of freedom ν and probability p(χ^2,ν) of exceeding χ^2. These χ^2 values are used to test the significance of the best-fitting models (third p column) and to derive error bars for the free parameters of these best-fitting models (ν = 3).

			p	
	1σ	2σ		3σ
ν	0.683	0.954	0.99	0.9973
1			6.64	
2			9.21	
3	3.53	8.02	11.3	14.2
4			13.3	
5			15.1	

however, lay in the field of the, above mentioned, assumptions which put constraints on the number of free parameters of the curve of growth models.

7.2. IR colours of γ Cas

To get an indication of what results we may expect when using the IR data of γ Cassiopeiae to derive the density structure parameters of the envelope, we constructed a colour-colour diagram in which observed and theoretical colours are plotted. According to Waters (1986) the partially optically thick region of the curve of growth models can be approximated by

$$\log\left(Z_\nu - 1\right) = \frac{2}{2n-1}\log\left(2C_{n,\theta}E_\nu\right) + A_n \qquad (7)$$

where n is the exponent of the density law (Eq. (1)) and θ the opening angle of the disc-like envelope. Therefore the ratio of two excess fluxes at different wavelengths can be written as

$$\log\left(\frac{Z_{\nu_1}-1}{Z_{\nu_2}-1}\right) = \frac{2}{2n-1}\log\left(\frac{X_{\lambda_1}}{X_{\lambda_2}}\right). \qquad (8)$$

If $Z_\nu \gg 1$ then Eq. (8) can be written as

$$\log\left(\frac{Z_{\nu_1}}{Z_{\nu_2}}\right) = \frac{2}{2n-1}\log\left(\frac{X_{\lambda_1}}{X_{\lambda_2}}\right) \qquad (9)$$

with X_λ defined as in Eq. (5). The difference in brightness of a star at two wavelengths is given by

$$\begin{aligned} m_{\lambda_1} - m_{\lambda_2} &= 2.5\log\left(\frac{F_{\nu_2}}{F_{\nu_1}}\right) + 2.5\left(C_{\lambda_1} - C_{\lambda_2}\right) \\ &= 2.5\log\left(\frac{Z_{\nu_2}F_{\nu_2,*}}{Z_{\nu_1}F_{\nu_1,*}}\right) + 2.5\left(C_{\lambda_1} - C_{\lambda_2}\right) \end{aligned} \qquad (10)$$

where $F_{\nu,*}$ represents the photospheric flux and with C_λ as listed in Table 2. Hence, IR colours predicted by COG models are given by

$$\begin{aligned} m_{\lambda_1} - m_{\lambda_2} = \frac{5}{2n-1}\log\left(\frac{X_{\lambda_2}}{X_{\lambda_1}}\right) &+ 2.5\log\left(\frac{F_{\nu_2,*}}{F_{\nu_1,*}}\right) \\ &+ 2.5\left(C_{\lambda_1} - C_{\lambda_2}\right), \end{aligned} \qquad (11)$$

(combining Eqs. (9) and (10)). Hence, if the excesses $(Z_{\nu_1} - 1)$ and $(Z_{\nu_2} - 1)$ lie within the partially optically thick region of the curve of growth model, the theoretical colours do not depend on the opening angle or the radius of the disc.

Figure 6 displays a M−N versus K−L colour-colour diagram of the data of γ Cas. The plotted colours are derived from the IR data in Table 1. The straight lines in Fig. 6 represent, the above mentioned, theoretical colour calculations (Eq. (11)) for different values of n. The solid line is found when adopting a Kurucz (1979) model with parameters $T_{\rm eff}$ = 30000 K and $\log g$ = 3.5 to define the photospheric flux of γ Cas. The dashed line is found when using the Kurucz model with $T_{\rm eff}$ = 22500 K and $\log g$ = 3.0. For the calibration constants C_λ we used the values of the WIRO calibration as listed in Table 2. Figure 6 clearly shows that values of $n < 2$, corresponding to infall of envelope matter, are not likely to be found when fitting spherical or disc-like curve of growth models to the IR data. Furthermore, most of the data indicate a rather constant value of n $\approx$ 3.0.

7.3. Fitting COG models to the IR data of γ Cas

The IR data of γ Cas are reduced to excess fluxes, as described in Sect. 6. After calculating the value of X_λ for the IR data, using Eq. (5), the COG models can be fitted to these values. We applied an opening angle of 15 degrees to the models and fitted a grid of models with $1.5 \leq n \leq 4.0$ and $2.86 \leq R_{\rm disc}/R_* \leq 1000$ to the IR data of γ Cas (Table 1). For each data set we minimized the fit quality of the models on each grid point by using the χ^2 technique, i.e. we shifted the models horizontally in the $\log(Z_\nu - 1)$ versus $\log(E_\nu)$ diagram until the lowest value of χ^2 was found. The model on the grid point with lowest χ^2 value was adopted as best-fitting COG model.

We show two examples of the results of the fitting procedure in Fig. 7. In this figure the best-fitting COG model for two IR data sets is plotted. Uncertainties of the IR observations are indicated with 1σ error bars. Figure 7 also displays the resulting energy distributions of these models together with the UV and IR photometry. The Kurucz models are represented by a solid line, and the computed energy distribution of Kurucz+COG model is represented by a dashed line. In addition Fig. 7 maps, for the considered data sets, the minimized χ^2 values in a $R_*/R_{\rm disc}$ versus n grid. The lowest χ^2 value over all grid points is indicated by an asterisk. To determine error bars for the best-fit value of n we plotted 1σ, 2σ and 3σ $\Delta\chi^2$ contours around the best fit. Table 4 lists these $\Delta\chi^2$ values. After drawing these contours, the error bars can be measured from the contour plots (for detailed description see e.g. Lampton et al. (1976) or Press et al. (1986)). This way of estimating errors implies that no error bars can be assigned to data sets with only three data points. This is due to the fact that the, above described, fitting technique is applied to models with three adjustable parameters (n, $R_{\rm disc}$ and X_*).

Table 5 lists the results of fitting COG models to the IR data. It includes derived visual excess ratios, fluxes and magnitudes. These properties are derived by extrapolating the best fitting COG models to the visual wavelength λ=550 nm. The model

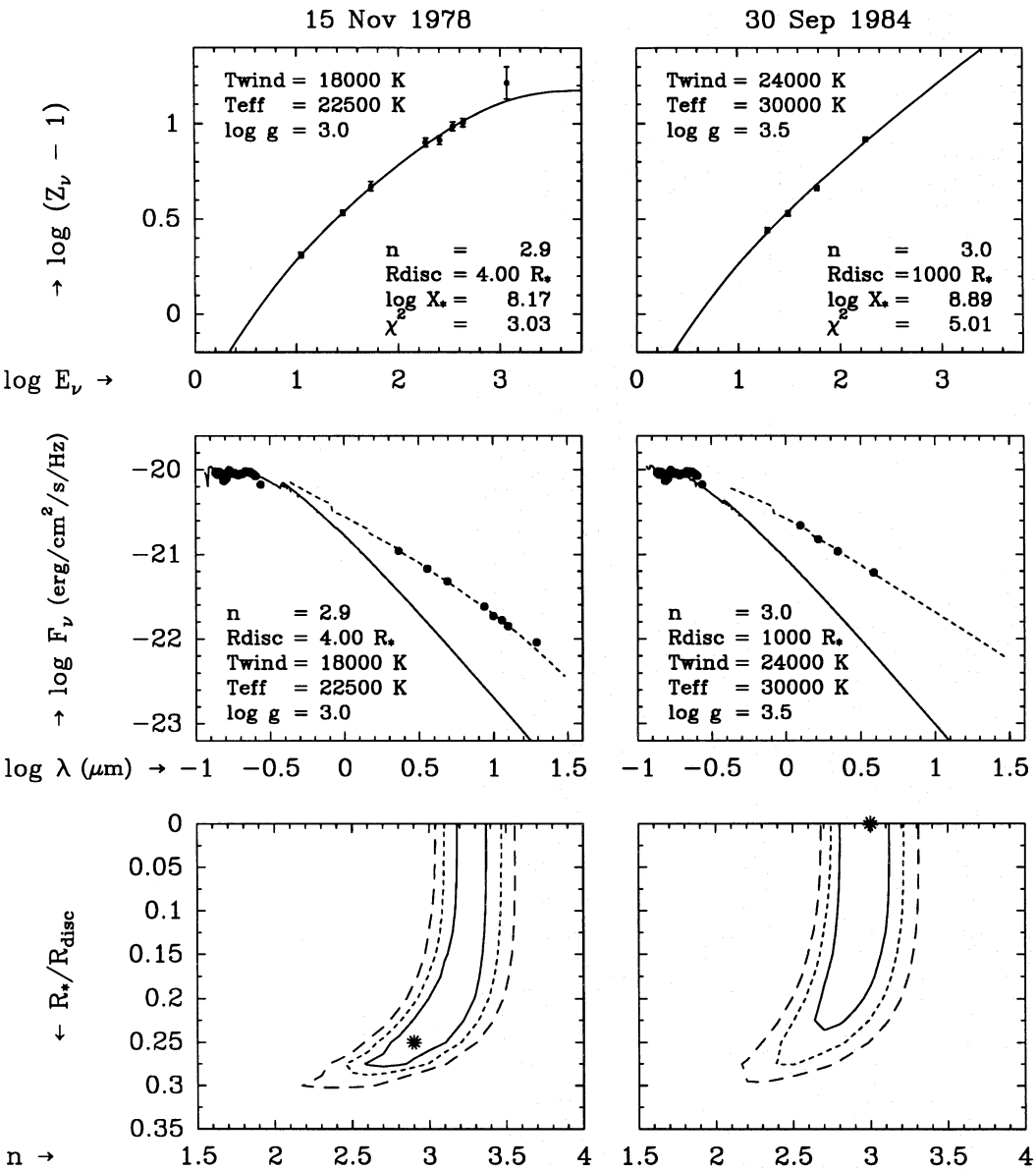

Fig. 7. Left) Sample plot of the results of fitting curve of growth models to IR data. Adopted stellar parameters : $\log g = 3.0$, $T_{\rm eff} = 22500$ K. For each IR data set three panels are plotted. **Top** Best fitting COG model with IR data. Uncertainties of the IR data are indicated with 1σ error bars. **Middle** Energy distribution of Kuruçz model and best fitting COG model. The Kurucz model is plotted as a solid line. The energy distribution of Kurucz+COG model is represented by a dashed line. S2/68 UV continuum fluxes and the IR fluxes are also displayed. **Bottom** Quality of fits. The 1σ, 2σ and 3σ $\Delta\chi^2$ contours of fitting a grid of COG models to observed IR excesses are shown. The 1σ contour is represented by a solid line, the 2σ contour by a dotted line and the 3σ by a dashed line. We used a grid of COG models with n between 1.5 and 4.0 and with $R_{\rm disc}$ ranging from 2.86 R_* to 1000 R_*. The best fitting models are indicated by an asterisk. **Right)** As Left) for a different IR data set. Adopted stellar parameters: $\log g = 3.5$, $T_{\rm eff} = 30000$ K

predicts the excess ratio Z_V, which is converted to the flux of star+disc by multiplying by the photospheric Kurucz flux. Visual magnitudes are calculated using

$$m_V = 2.5 * (C + \log F_{\rm Kur}(550)) \ , \qquad (12)$$

where C=19.436 (Landolt-Börnstein 1982).

For all data sets with more than 3 data points, we tested if the best-fitting model is able to fit the data within a 99% significance level. Table 4 lists the χ^2 levels we used for this test. The number of degrees of freedom ν is defined as $\nu = N_{\rm obs} - N_{\rm par}$ (Lampton et al. 1976), where $N_{\rm obs}$ is the number of observations in a data set and $N_{\rm par}$ is the number of free parameters of the model (in this case $N_{\rm par} = 3$). Results of this test can be found in Table 5.

From Fig. 7 it becomes clear that the values of the disc radius we find are very sensitive to far IR measurements. Since a considerable fraction of the far IR excess is emitted at the outer regions of the disc, one needs observations in this wavelength

Table 5. Results of fitting COG models to the IR data. The N_{obs} column gives the number of different IR wavelengths in the data sets. Columns 3, 4, and 5 specify the derived COG model parameters n, R_{disc}, and log X_* respectively. Column 6 gives the χ^2 value of the best fits. Models that can not fit the data within a 99% significance level, are marked with an *. Columns 7–9 list the derived visual excess ratio, flux and magnitude. **Top section)** Results based on the representation of the photospheric flux by a Kurucz model with parameters T_{eff} = 22500 K and log g = 3.0. **Bottom section)** As top but based on a Kurucz model with parameters T_{eff} = 30000 K and log g = 3.5.

date	N_{obs}	n	R_*/R_{disc}	log X_*	χ^2	$Z_V - 1$	log F_V	m_V	
Oct 13 63	3	4.0	0.350	8.31	6.02	0.22	−20.28	2.10	
Nov 04	3	4.0	0.350	8.17	6.90	0.17	−20.30	2.15	
Dec 16	3	4.0	0.350	8.38	12.11	0.25	−20.27	2.07	
Dec 13 64	3	3.8	0.025	8.41	0.16	0.30	−20.25	2.04	
Dec 22	3	3.5	0.001	8.09	10.77	0.18	−20.29	2.14	
1971	3	2.4	0.001	7.67	0.51	0.16	−20.30	2.16	
1972–1973	8	2.7	0.175	7.84	6.15	0.17	−20.29	2.15	
Jun 24 78	7	3.2	0.300	8.16	*13.86	0.24	−20.27	2.08	
Jun 25	7	3.1	0.275	8.15	13.00	0.25	−20.27	2.07	
Aug 24	7	3.3	0.150	8.38	5.85	0.37	−20.23	1.98	
Sep 21	4	2.8	0.325	8.10	0.55	0.27	−20.26	2.06	
Oct 15	7	3.3	0.175	8.32	2.16	0.32	−20.24	2.01	Stellar parameters:
Nov 15	8	2.9	0.250	8.17	3.03	0.30	−20.25	2.03	T_{eff} = 22500 K
Sep 03 79	7	3.1	0.175	8.19	10.85	0.28	−20.26	2.05	log g = 3.0
Dec 28	7	2.5	0.125	7.84	*13.59	0.21	−20.28	2.11	$F_{Kur}(550)$ = −20.363
Aug 21 80	8	3.1	0.001	8.13	*36.55	0.24	−20.27	2.08	
Sep 27	8	2.9	0.125	7.99	*17.00	0.21	−20.28	2.12	
Oct 01	3	3.7	0.050	8.25	0.25	0.22	−20.28	2.10	
Sep 30 81	5	3.0	0.001	8.03	*12.91	0.21	−20.28	2.11	
1983	3	3.0	0.150	8.05	0.01	0.22	−20.28	2.10	
Sep 14 83	4	3.0	0.125	8.24	0.94	0.33	−20.24	2.01	
Sep 20	4	2.6	0.001	7.87	*8.22	0.21	−20.28	2.11	
Sep 30 84	4	3.0	0.001	8.13	4.33	0.26	−20.26	2.07	
Sep 29 86	4	1.7	0.350	7.52	22.28	0.18	−20.29	2.14	
Nov 27	4	1.5	0.350	7.45	8.09	0.19	−20.29	2.13	
Nov 25 88	5	2.9	0.001	8.13	6.32	0.28	−20.26	2.05	
Oct 13 63	3	4.0	0.350	9.38	1.52	1.16	−20.27	2.09	
Nov 04	3	4.0	0.350	9.26	4.36	0.99	−20.31	2.17	
Dec 16	3	4.0	0.350	9.44	2.88	1.25	−20.25	2.04	
Dec 13 64	3	3.6	0.175	9.26	0.09	1.23	−20.26	2.05	
Dec 22	3	3.6	0.001	9.08	10.72	0.95	−20.32	2.20	
1971	3	2.5	0.001	8.35	0.89	0.57	−20.41	2.43	
1972–1973	8	2.7	0.125	8.50	5.30	0.62	−20.39	2.39	
Jun 24 78	7	2.9	0.225	8.73	12.39	0.82	−20.34	2.27	
Jun 25	7	3.0	0.200	8.85	10.93	0.95	−20.31	2.19	
Aug 24	7	3.2	0.150	9.15	6.33	1.33	−20.24	2.00	
Sep 21	4	2.8	0.225	8.79	1.06	0.99	−20.31	2.18	
Oct 15	7	3.2	0.150	9.08	2.60	1.21	−20.26	2.06	Stellar parameters:
Nov 15	8	2.9	0.175	8.89	3.69	1.10	−20.28	2.12	T_{eff} = 30000 K
Sep 03 79	7	3.0	0.150	8.89	10.67	1.03	−20.30	2.15	log g = 3.5
Dec 28	7	2.5	0.100	8.44	12.02	0.67	−20.38	2.36	$F_{Kur}(550)$ = −20.604
Aug 21 80	8	3.1	0.001	8.91	*39.73	0.99	−20.31	2.17	
Sep 27	8	2.9	0.100	8.71	*16.28	0.80	−20.35	2.28	
Oct 01	3	3.6	0.001	9.14	0.52	1.04	−20.30	2.15	
Sep 30 81	5	3.0	0.001	8.79	*13.86	0.85	−20.34	2.25	
1983	3	2.9	0.100	8.65	0.02	0.71	−20.37	2.34	
Sep 14 83	4	3.1	0.001	9.10	0.46	1.34	−20.24	2.00	
Sep 20	4	2.7	0.001	8.61	*13.08	0.78	−20.35	2.30	
Sep 30 84	4	3.0	0.001	8.89	5.01	1.02	−20.30	2.16	
Sep 29 86	4	1.7	0.275	8.00	*13.15	0.54	−20.42	2.45	
Nov 27	4	1.8	0.250	8.05	5.17	0.56	−20.41	2.44	
Nov 25 88	5	2.9	0.001	8.86	6.57	1.05	−20.29	2.14	

region to put constraints on the size of the envelope. Luckily, γ Cas is observed with the IRAS satellite. These measurements give a lower limit for the disc radius of $R_{disc} \approx 6.7\,R_*$ (see Table 5) at the time of the IRAS observations (1983). For most of the other IR data sets listed in Table 1, the derived values of R_{disc} have, due to the lack of far IR data, very large 1σ errors. Waters et al. (1991) find, based on mm and cm observations, that the envelope of the star extends to at least 33 stellar radii. If the envelope of γ Cas was as large as this during the period studied in this paper, the disc radii derived here should be considered as lower limits.

Figure 8 shows in different panels the history of the V/R ratio of the Hβ emission line of γ Cas and the derived exponent of the density law of the equatorial disc (i.e. parameter n) for all data sets with χ^2 fit qualities within 99% significance. Derived 1σ error bars are indicated. Figure 8 clearly shows that the value of n is variable. Although we find for one IR dataset a value of $n < 2$ (in the case of T_{eff} = 22500 K), which might suggest infall of matter, we do not see a correlation between the measured V/R variability and the deduced values of n. The IR dataset which suggests infall is indeed collected at times of a high V/R ratio. However, at other epochs of high V/R values we find values of $n \approx 3$. Therefore a correlation between V/R variability and the radial density structure of the envelope of γ Cas seems unlikely. Since we believe that the IR excess and the Balmer Hβ emission line are formed in the same wind region of the star, we have to conclude that the expanding/contracting envelope model, which is used to explain the V/R variations of Be stars, is inconsistent with our IR data.

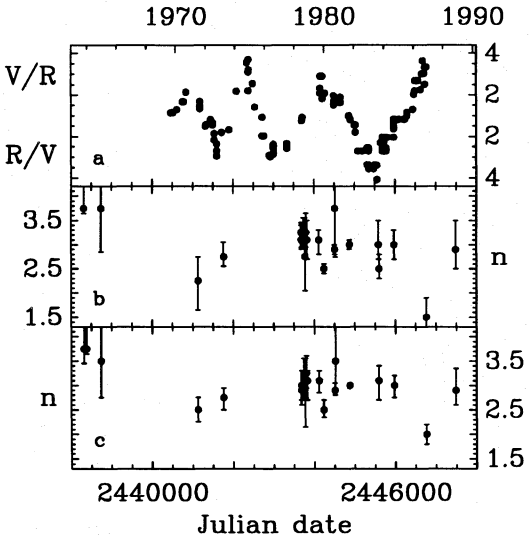

Fig. 8. **a)** V/R behaviour of γ Cas. **b)** Derived exponent of density law for all data sets with fit qualities within acceptable significance. We have indicated 1σ error bars. Stellar parameters: $\log g$ = 3.0, T_{eff} = 22500 K. **c)** As b) with stellar parameters $\log g$ = 3.5 and T_{eff} = 30000 K

8. Discussion and conclusions

We have investigated the long-term variation in the density structure of the envelope of γ Cassiopeiae to see if there is any correlation between the radial density structure and the V/R variability. We used the curve of growth model to interpret our infrared data of γ Cas. In the following we discuss our results and we summarize the conclusions we make according to the results we presented in the preceding sections.

We used the value E(B−V) = 0.03 to correct the ultraviolet and infrared observations of γ Cas for interstellar extinction. The ultraviolet flux of γ Cas as measured by the S2/68 telescope can not be ideally described by a Kurucz model. This is probably due to the shape of the intrinsic energy distribution of γ Cas. Adopting a different value for E(B−V) might result in finding a better fitting Kurucz model to represent the photospheric flux of the star.

A comparison of the UV energy distribution of γ Cas with the UV energy distributions of two other B0.5 type stars shows that the slope of the energy distribution of γ Cas is much flatter than the slopes of the distributions of the comparison stars (see Fig. 8). If we assume that the three stars have the same photospheric effective temperature, the difference in slope could be due to a flux contribution of material surrounding the star. The colour-colour diagram plotted in Fig. 3 indicates that the far IR spectrum of γ Cas cannot be represented by a blackbody energy distribution alone, and that a power law energy distribution fits these data much better. The power of this energy distribution can be understood in terms of free-free and bound free emission from circumstellar material that contributes to the total flux.

The accuracy of the adopted value of E(B−V) affects the accuracy of our results. Errors in the determination of the excess fluxes are given by

$$\mathrm{d}\,(\log(Z_\lambda - 1)) = \frac{Z_\lambda}{Z_\lambda - 1}\,\{\mathrm{d}\,(\log F_\lambda) - \mathrm{d}\,(\log F_*)\}$$

where d(log F_λ) is the error of the observed flux at wavelength λ and where d(log F_*) is the error in the derived photospheric flux. The latter value should be the same for all wavelengths if the Kurucz models are perfect. Possible wrong calibration of the S2/68 fluxes and, more important, an error in the value of E(B−V), make the error d(log F_*) much larger than the error of any of the individual observations. From calculations we find that an error of, for instance, d(E(B−V) = 0.03 means that d(log F_*) $\approx$ 0.1, which is over 10 times the inaccuracy in the individual ultraviolet and infrared observations. The errors we used for the χ^2 tests to fit the curve of growth models to the infrared data of γ Cas are the errors of the individual infrared observations only. Applying an additional unknown error d(log F_*) to the data, would give better χ^2 values for the best-fitting curve of growth models (Table 5). Hence, to test the significance of the best-fitting curve of growth models, it is very important that the correct values of E(B−V) and d(E(B−V)) in the direction of γ Cas are known.

We stress however that the derived values of the density structure parameter n, *do not depend on the adopted value of E(B−V)*. This density parameter only depends on the slope of the IR energy distribution and the slope of the photospheric energy

distribution, which are not sensitive to the use of different values for the interstellar extinction correction. When applying higher values of E(B−V) the actual excesses will increase and thus one will find larger disc radii and higher values of log X_* , i.e. higher densities at the base of the disc.

The density gradient, parameter n, of the envelope of γ Cas turns out to be variable, but not in a way that can explain the V/R variability: it is concentrated around the value $n = 3$ and only one value of $n < 2$ (which could mean inflow, V/R>1) within a 99% significance level is found. Figures 8a–8c indicate that any relation between density structure and Hβ V/R variation seems very unlikely. Figures 1b–1d also show no obvious relation between the Hβ V/R behaviour and the K fluxes or K−L colour of γ Cas. Hence the V/R variation in emission lines does not seem to originate from a long time scale variation in the density structure of the low-velocity, high-density, disc-like wind. It is believed, however, that the Hβ emission line and the IR excess are formed in the same region of the envelope. We conclude that it is difficult to understand the IR data when adopting the expansion/contraction model. Because the IR data of γ Cas are more consistent with the disc model, we find the model proposing a rotating non-axisymmetric disc the most favourable of the two considered models. The continuum energy distribution is not very sensitive to deviations in the axisymmetry, while the line shapes clearly are. Therefore we believe that γ Cas is surrounded by a high-velocity, low-density non-equatorial wind, which accounts for several UV spectral features, together with a low-velocity, high-density, disc-like structure in which the IR and far IR excess are caused by free-free and free-bound emission.

Adopting different Kurucz models, which represent the photospheric flux, did not change the results of our analysis. This is due to the fact that the slopes of the energy distribution of both used Kurucz models are practically the same at IR wavelengths. Therefore the deduced values of n do not differ much when adopting different Kurucz models.

In our analysis we assumed the UV flux of γ Cas to be constant. Although the derived values of the density structure parameter n would not change significantly if the UV flux would be slightly variable, we expect the accuracy of the derived parameters X_* and R_{disc} to depend strongly on the absolute ultraviolet continuum fluxes measured by the S2/68 telescope. Since UV continuum observations of γ Cas are made only before and at the time the ESRO satellite, carrying the S2/68 telescope, was operating, a check on the constancy of these fluxes would be wishful (this of course implying new observations). We might be able to check the UV variability of γ Cas in a forthcoming investigation on UV spectral line characteristics of γ Cas. For this research programme we will use high-resolution UV spectra collected with the International Ultraviolet Explorer satellite.

Acknowledgements. The research of LBFMW has been made possible by a fellowship of the Royal Netherlands Academy of Arts and Sciences.

References

Allen, D.A.: 1973, MNRAS, 161, 145
Ashok, N.M., Bhatt, H.C., Kulkarni, P.V., Joshi, S.C.: 1984, MNRAS, 211, 471
Böhme, D.: 1985, IAU Inf. Bull. Var. Stars 2723
Böhme, D.: 1986, IAU Inf. Bull. Var. Stars 2893
Clark, D.: 1990, A&A, 227, 151
Cowley, A.P., Rogers, L., Hutchings, J.B.: 1976, PASP, 88, 911
Dachs, J., Hanuschik, R., Kaiser, D., Rohe, D.: 1986, A&A, 159, 276
Dachs. J.: 1987, in: IAU Colloquium 92, Physics of Be stars, ed. A. Slettebak and T.P. Snow, Cambridge University Press, p. 150
Dachs, J., Engels, D., Kiehling, R.: 1988, A&A, 194, 167
Doazan, V.: 1982, in: B stars with and without emission lines, ed. A.B. Underhill and V. Doazan, NASA SP-456, p. 325
Doazan, V., Franco, M., Rusconi, L., Sedmak, G., Stalio, R.: 1984, A&AS, 55, 1
Doazan, V., Rusconi, L., Sedmak, G., Thomas, R.N., Bourdonneau, B.: 1987, A&A, 182, L25
Doazan, V.: 1987, in: IAU Colloquium 92, Physics of Be stars, ed. A. Slettebak and T.P. Snow, Cambridge University Press, p. 384
Ferrari-Toniolo, M., Persi, P., Viotti, R.: 1978, MNRAS, 185, 841
Frontera, F., Dal Fiume, D., Robba, N.R., Manzo, G., Re, S., Costa, E.: 1987, ApJ, 320, L127
Gehrz, R.D., Hackwell, J.A., Jones, T.W.: 1974, ApJ, 191, 675
Goraya, P.S., Tur, N.S.: 1988, Ap&SS, 145, 263
Hammerschlag-Hensberge, G.: 1979, IAU Circ. 3391
Henrichs, H.F., Hammerschlag-Hensberge, G., Howarth, I.D., Barr, P.: 1983, ApJ, 268, 807
Hoffleit, D., Jaschek, C.: 1982, The Bright Star Catalogue, Yale University Observatory
Howarth, I.D.: 1979, Journal of the Brit. Astron. Assoc., 89, 378
Huang, S.-S.: 1972, ApJ, 171, 549
Johnson, H.L., Mitchell, R.I., Iriarte, B., Wisniewski, W.Z.: 1966, Comm. Lunar Planet. Lab., 4, 99
Jones, T.J.: 1979, ApJ, 228, 787
Koornneef, J.: 1983, A&A, 128, 84
Kurucz, R.L.: 1979, ApJS, 40, 1
Lamers, H.J.G.L.M., Waters, L.B.F.M.: 1984, A&A, 136, 37
Lampton, M., Margon, B., Bowyer, S.: 1976, ApJ, 208, 177
Landolt-Börnstein: 1982, Numerical data and functional relationships in science and technology, new series, group VI, volume 2B
Lesh, J.R.: 1968, ApJS, 17, 371
Lowe, R.P., Moorhead, J.M., Wehlau, W.H., Barker, P.K., Marlborough, J.M.: 1985, ApJ, 290, 325
Macau-Hercot, D., Jamar, C., Monfils, A., Thompson, G.I., Houziaux, L., Wilson, R.: 1978, Supplement to the ultraviolet bright-star spectrophometric catalogue, ESA SP 28
Marlborough, J.M.: 1977, PASP, 89, 122
Marlborough, J.M., Snow, T.P., Slettebak, A.: 1978, ApJ, 224, 157
Mourard, D., Bosc, I., Labeyrie, A., Koechlin, L., Saha, S.: 1989, Nat, 342, 520
Murakami, T., Koyama, K., Inoue, H., Agrawal, P.C.: 1986, ApJ, 310, L31
Okazaki, A.T.: 1991, PASJ, 43, 75
Olnon, F.M.: 1975, A&A, 39, 217
Panagia, N., Felli, M.: 1975, A&A, 39, 1
Persi. P., Ferrari-Toniolo, M., Shivanandan, K., Ranieri, M., Marenzi, A: 1990, A&A, 237, 153

Persi, P., Tapia, M., Rodriquez, L.F., Ferrari-Toniolo., M., Roth, M: 1990, A&A, 240, 93
Poeckert, R., Marlborough, J.M.: 1977, ApJ, 218, 220
Poeckert, R., Marlborough, J.M.: 1978, ApJ, 220, 940
Press, W.H., Flannery, B.P., Teukolsky, S.A., Vetterling, W.T.: 1986, Numerical recipes, Cambridge University Press
Savage, B.D., Mathis, J.S.: 1979, ARA&A, 17, 84
Scargle, J.D., Erickson, E.F., Whitteborn, F.C., Strecker, D.W.: 1978, ApJ, 224, 527
Secchi, A.: 1867, Astron. Nachr., 68, 63
Slettebak, A., Snow, T.P.: 1978, ApJ, 224, L127
Slettebak, A.: 1982, ApJS, 50, 55
Slettebak, A.: 1988, PASP, 100, 770
Sobolev, V.V.: 1960, Moving envelopes of stars, Harvard University Press
Struve, O.:1931, ApJ, 73, 94
Telting, J.H., Waters, L.B.F.M., Persi, P., Dunlop, S.: 1991, in: ESO Workshop on Rapid Variability of OB Stars: Nature and Diagnostic Value, ed. D. Baade, ESO Proceedings no. 36, 57
Waters, L.B.F.M.: 1986, A&A, 162, 121
Waters, L.B.F.M., Coté, J., Lamers, H.J.G.L.M.: 1987, A&A, 185, 206
Waters, L.B.F.M., van der Veen, W.E.C.J., Taylor, A.R., Marlborough, J.M., Dougherty, S.M.: 1991, A&A, 244, 120
White, N.E., Swank, T.P., Holt, S.S., Parmar, A.N.: 1982, ApJ, 263, 277
Wright, A.E., Barlow, M.J.: 1975, MNRAS, 170, 41
Yang, S., Ninkov, Z., Walker, G.A.H.: 1988, PASP, 100, 233

This article was processed by the author using Springer-Verlag LaTeX A&A style file version 3.